Application of *T*-matrix method in solving mixed boundary separable obstacle problem

Xiuzhu Ye,[1,*] Rencheng Song,[2] and Xudong Chen[2]

[1]*Department of Electrical and Computer Engineering, Beihang University, Beijing 100191, China*
[2]*Department of Electrical and Computer Engineering, National University of Singapore, 117576, Singapore*
**yexiuzhu@buaa.edu.cn*

Abstract: The practical problem of imaging scatterers enclosed by separable obstacles with mixed boundary is addressed. Both the unknown scatterers and the known obstacle media can be mixture of dielectric and perfect electric conducting (PEC) materials. The scattering phenomenon of such problem is well modeled by *T*-matrix method. By usage of *separable* prior information, the obstacle media are treated as known scatterers rather than part of the background. The number of unknowns is thus reduced greatly. After recovering the profiles of scatterers by *T*-matrix method, a criterion is further provided to classify the PEC and dielectric scatterers. Various numerical examples are presented to show the effectiveness and good performance of the method.

OCIS codes: (290.3200) Inverse scattering; (180.6900) Three-dimensional microscopy.

References and links

1. M. A. Fiddy and M. Testorf, "Inverse scattering method applied to the synthesis of strongly scattering structures," Opt. Express **14**(5), 2037–2046 (2006).
2. P. C. Chaumet, K. Belkebir, and R. Lencrerot, "Three-dimensional optical imaging in layered media," Opt. Express **14**(8), 3415–3426 (2006).
3. S. He, L. Zhuang, F. Zhang, W. Hu, and G. Zhu, "Investigation of range profiles from buried 3-D object based on the EM simulation," Opt. Express **19**(13), 12291–12304 (2011).
4. J. Shen, X. Chen, Y. Zhong, and L. Ran, "Inverse scattering problem in presence of a conducting cylinder," Opt. Express **19**(11), 10698–10706 (2011).
5. A. Logvin, L. Ligthart, and A. Kozlov, "Methods for solving inverse problems in radar remote sensing," in Mikon-2002: Xiv International Conference on Microwaves, Radar and Wireless Communications," Proceedings **1–3**, 681–685 (2002).
6. A. Massa, M. Pastorino, A. Rosani, and M. Benedetti, "A microwave imaging method for NDE/NDT based on the SMW technique for the electromagnetic field prediction," IEEE Trans. Instrum. Meas. **55**(1), 240–247 (2006).
7. M. Benedetti, M. Donelli, and A. Massa, "Multicrack detection in two-dimensional structures by means of GA-based strategies," IEEE Trans. Antenn. Propag. **55**(1), 205–215 (2007).
8. X. Chen, "Subspace-based optimization method for inverse scattering problems with an inhomogeneous background medium," Inverse Probl. **26**(7), 074007 (2010).
9. L. Song, C. Yu, and Q. Liu, "Through-wall imaging (TWI) by radar: 2-D tomographic results and analyses," IEEE Trans. Geosci. Rem. Sens. **43**(12), 2793–2798 (2005).
10. A. Devaney and R. Porter, "Holography and the inverse source problem. II. Inhomogeneous media," J. Opt. Soc. Am. A **2**(11), 2006–2012 (1985).
11. J. M. Tualle, J. Prat, E. Tinet, and S. Avrillier, "Real-space Green's function calculation for the solution of the diffusion equation in stratified turbid media," J. Opt. Soc. Am. A **17**(11), 2046–2055 (2000).
12. A. Abubakar, W. Hu, P. M. van den Berg, and T. M. Habashy, "A finite-difference contrast source inversion method," Inverse Probl. **24**(6), 065004 (2008).
13. X. Ye, R. Song, K. Agarwal, and X. Chen, "Electromagnetic imaging of separable obstacle problem," Opt. Express **20**(3), 2206–2219 (2012).
14. X. Ye, X. Chen, Y. Zhong, and R. Song, "Simultaneous reconstruction of dielectric and perfectly conducting scatterers via T-matrix method," IEEE Trans. Antenn. Propag. **61**(7), 3774–3781 (2013).
15. M. I. Mishchenko, L. Liu, D. W. Mackowski, B. Cairns, and G. Videen, "Multiple scattering by random particulate media: exact 3D results," Opt. Express **15**(6), 2822–2836 (2007).
16. M. I. Mishchenko, L. Liu, and G. Videen, "Conditions of applicability of the single-scattering approximation," Opt. Express **15**(12), 7522–7527 (2007).
17. S. H. Simpson and S. Hanna, "Application of the discrete dipole approximation to optical trapping calculations of inhomogeneous and anisotropic particles," Opt. Express **19**(17), 16526–16541 (2011).

#210984 - $15.00 USD Received 28 Apr 2014; revised 13 Jun 2014; accepted 14 Jun 2014; published 24 Jun 2014

18. G. Otto, W. Chew, "Microwave inverse scattering - local shape function imaging for improved resolution of strong scatterers," IEEE Trans. Microw. Theory **42**(1), 137–141 (1994).
19. G. Otto and W. Chew, "Inverse Scattering of H-Z Waves using local shape-function imaging - a T-Matrix formulation," Int. J. Imaging Syst. Technol. **5**(1), 22–27 (1994).
20. J. Lin and W. Chew, "Solution of the three-dimensional electromagnetic inverse problem by the local shape function and the conjugate gradient fast Fourier transform methods," J. Opt. Soc. Am. A **14**(11), 3037–3045 (1997).
21. W. Chew, *Waves and Fields in Inhomogeneous Media* (Van Nostrand Reinhold, 1990).
22. T. Rao and X. Chen, "Analysis of the time-reversal operator for a single cylinder under two-dimensional settings," J. Electromagn. Wave **20**(15), 2153–2165 (2006).

1. Introduction

Inverse scattering problems are of great interests to scientists nowadays [1–4]. It has a wide application in the fields of optical diffraction tomography [2], remote sensing [5] and non-destructive evaluation [6, 7], etc. Among various inverse scattering problems, the inhomogeneous background detections [3, 8–12] are of particular interest due to their practical applications in biomedical imaging, through wall imaging and geophysical detection. A special kind of inhomogeneous background detection problem is called separable obstacle problem (SOP). It refers to the inverse scattering problem where the unknown scatterers are enclosed by known background media/obstacles that are *non-overlap* with them. The SOPs are encountered very often in practice. The quality evaluation of cores in optical fibers is a typical SOP. Some through wall imaging problems can also be classified as SOP, such as detecting the furniture/humans inside a room, inspecting the contents of closed parcels in standard shipment packages and imaging the contents of storage tanks, etc. Traditional techniques dealing with inhomogeneous background detections [3, 8] usually treat the obstacle media as part of the inhomogeneous background, which involve the cumbersome numerical calculation of the inhomogeneous background Green's function. Recently, a different method called separable obstacle problem-homo (SOP-homo) [13] has been specially proposed to solve the SOP. It has been verified that by usage of the *separable* information of the obstacles, the SOP-homo cannot only employ the analytical Green's function in homogeneous background, but also reduce the number of unknowns involved in the reconstruction process.

In [13], the obstacles and the scatterers are both known to be dielectrics implicitly. However, in practice, the obstacle media can be composed by both the wave penetrable (i.e. dielectric) material and impenetrable (i.e., PEC) material simultaneously. For example, the concrete walls are embedded with reinforcing steel bars inside, or the storage tanks are composed by both wood and metal. On the other hand, the scatterers enclosed by the obstacle can also be mixture of PEC and dielectric [14]. Therefore, there is an urgent need to simultaneously reconstruct PEC and dielectric materials together in SOP.

As the boundary conditions for dielectric and PEC materials are different, we define the SOP which involves both kinds of materials together as the mixed boundary SOP (MB-SOP). And it is the target of the present study. As a special kind of SOP, the *separable* information of the obstacle and the unknown targets is still known *a priori* in MB-SOP. The parameters to be determined in MB-SOP are the shapes for the PEC scatterers and the spatial distribution of the relative permittivities for the dielectric scatterers. There are three main challenges for solving MB-SOP. Firstly, a unified modeling method is needed to describe the scattering effect of PEC and dielectric together. Secondly, a classification criterion is needed to recover the physical properties of the scatterers, which is the premise to further obtain their corresponding physical parameters. Thirdly, a combination of the new modeling method with the framework of SOP-homo method is needed.

For MB-SOP, we indicate that the method of moment (MoM) is not the best candidate for modeling. Due to the different boundary conditions, the scattering effect of dielectric scatterer is governed by volume integral equation while that of PEC is governed by the surface integral equation. Thus in MoM, the discritization methods and representations of basic elements are essentially different for the two kinds of scatterers. Recently, a *T*-matrix based inversion method [14] is proposed to solve the general mixed boundary inverse problem. In [14], the

#210984 - $15.00 USD Received 28 Apr 2014; revised 13 Jun 2014; accepted 14 Jun 2014; published 24 Jun 2014

scattered and incident fields are firstly expanded as functions of multipoles, and then coefficient of scattered field is related to that of incident field by *T*-matrix only utilizing the boundary condition. Therefore, in *T*-matrix method, the PEC and dielectric scatterers can be uniformly discretized into volume pixels. The *T*-matrices for each pixel can be retrieved from the given scattered field. Thus, it is found that *T*-matrix method [15–20] also serves as a proper modeling method for MB-SOP.

In this article, the *T*-matrix method is employed as the modeling method to solve the MB-SOP. Different from [13] which is modeled by electric field integral equation (EFIE), the *T*-matrix method is a Green's function free method. The SOP-homo [13] is employed to combine with the *T*-matrix method, i.e., by utilizing the prior information of the separable obstacle, the mixed boundary obstacles are treated as 'known scatterers'. Therefore, the elements that corresponding to the obstacles can be excluded from the updating process of unknowns. The proposed *T*-matrix based SOP-homo is an easy-implemented and economic computational method for solving MB-SOP. The similarities and differences of the proposed *T*-matrix based SOP-homo and the original SOP-homo method will be further discussed in Section 3.3. Various numerical examples are presented in this article to show the efficiency of our method. To the best knowledge of the authors, there is no article published yet on the topic of mixed boundary inhomogeneous background detection. Thus the investigation of MB-SOP is of essential importance to the development of inhomogeneous background detection.

2. Forward problem

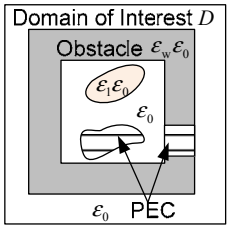

Fig. 1. A general scenario for mixed boundary separable obstacle problem (MB-SOP).

The general scenario of the MB-SOP is depicted in Fig. 1. Here we consider the two-dimensional setup with transverse magnetic wave illumination. The domain of interest is cylindrical which is invariant along the longitudinal direction, thus the transverse cross section can be used to depict the domain of interest. The experimental setup is as shown in Fig. 1: inside a given domain of interest D, the obstacle of relative permittivity ε_{w} is embedded with PEC rod inside. Unknown scatterers enclosed by obstacle can be either dielectric or PEC scatterers. There is no overlap between the obstacle and scatterers, and the information of the obstacle media is known *a priori*. We use N_{inc} time harmonic plane waves to symmetrically illuminate the domain of interest around a circle. Then the scattered field is collected by N_{r} receivers evenly distributed around a circle outside the domain of interest. Thus there are totally $N_{\mathrm{r}} \times N_{\mathrm{inc}}$ points of data recorded in the scattered field matrix.

We adopt the *T*-matrix method as the modeling scheme. The domain of interest is discretized into N square subunits and the number of subunits that belong to the obstacle is N_{w}. To use the analytical form of *T*-matrix for circles [21], the discretization should be fine enough such that the scattering behavior of each cell can be well approximated by a circle of the same area [19]. The equivalent radius of each subunit is R and their centers are located at $\boldsymbol{\rho}_i = (r_{0,i}, \theta_{0,i})$, $i = 1, 2, ..., N$, under the global coordinate system. The incident field can be expanded into multipoles series on each subunit. $\bar{\mathbf{e}}$ is vector of coefficients for the original

#210984 - $15.00 USD Received 28 Apr 2014; revised 13 Jun 2014; accepted 14 Jun 2014; published 24 Jun 2014

incident field with $\left[\mathbf{e}_i\right]_m = \mathrm{i}^m e^{\mathrm{i}k_0 r_{0,i}\cos(\theta_{0,i}-\theta_{\mathrm{inc}})} e^{-\mathrm{i}m\theta_{\mathrm{inc}}}$, $m=-M,...,M$. M is the truncation number of multipoles and θ_{inc} is the angle that the incident wave number makes with the global x-axis.

We are able to construct two matrix equations describing the scattering behavior of the scatterers [14]:

$$\overline{\mathbf{a}} = \overline{\overline{O}} \cdot \left[\overline{\mathbf{e}} - \overline{\overline{A}} \cdot \overline{\mathbf{a}} \right] \tag{1}$$

$$\mathbf{E}^{\mathrm{sca}} = \overline{\overline{\boldsymbol{\psi}}}^{\mathrm{t}} \cdot \overline{\mathbf{a}} \tag{2}$$

Equations (1) and (2) are referred as the state and the field equations respectively [8, 13]. Equation (1) is a self-consistent equation which relates the total electric field coefficients on each subunit to the scattered field coefficients by T-matrices. $\overline{\mathbf{a}}$ is the vector of amplitudes of induced multipoles. Diagonal matrix $\overline{\overline{O}}$ is the combination of all the T-matrices for each subunit, where $\overline{\overline{T}}_i$, $i=1,2,...,N$ are arranged along its diagonal. Matrix $\overline{\overline{A}}$ refers to the mapping that transfers the scattered field from other subunits into the incident field on the current subunit. In Eq. (2), $\overline{\overline{\boldsymbol{\psi}}}^{\mathrm{t}}$ denotes the mapping which maps the amplitudes of induced multipoles to the scattered field on receivers outside domain D. The detailed definition of other parameters in Eqs. (1) and (2) can be found in [14].

3. Inverse problem

Two processes are involved in solving the MB-SOP. The first process retrieves the T-matrices (matrix $\overline{\overline{O}}$) from the scattered field and will be introduced in section 3.1. The SOP-homo [13] combined with T-matrix inversion method [14] is adopted as the optimization scheme. After getting the reconstructed T-matrices, a second process is needed to classify the PEC from dielectric subunits, in order to further retrieve the physical properties for PEC and dielectric respectively. The classification criterion will be presented according to the analysis of monopole term in T-matrices in section 3.2.

3.1 The optimization procedure

3.1.1 The general *T*-matrix inversion method

The cost function for T-matrix inversion method [14] is consisted by both the residues in state equation and field equation. The residue in the field equation Δ^{fie} is given by the difference between the calculated and measured scattered field,

$$\Delta^{\mathrm{fie}} = \left\| \mathbf{E}^{\mathrm{sca}} - \overline{\overline{\boldsymbol{\psi}}}^{\mathrm{t}} \cdot \overline{\mathbf{a}} \right\|^2, \tag{3}$$

where $\|\cdot\|$ is the Euclidean length of a vector. The residue in the state equation is defined to be,

$$\Delta^{\mathrm{sta}} = \left\| \overline{\mathbf{a}} - \overline{\overline{O}} \cdot (\overline{e} - \overline{\overline{A}} \cdot \overline{\mathbf{a}}) \right\|^2. \tag{4}$$

Then the cost function with a single incidence is constructed as the summation of both the residues,

$$\Delta^{\mathrm{tot}} = \Delta^{\mathrm{fie}} / \left\| \overline{E}^{\mathrm{sca}} \right\|^2 + \Delta^{\mathrm{sta}} / \left\| \overline{\mathbf{a}}^{\mathrm{s}} \right\|^2. \tag{5}$$

where $\overline{\mathbf{a}}^{\mathrm{s}}$ is the deterministic part of $\overline{\mathbf{a}}$ that is uniquely defined by the scattered field and the singular values of mapping $\overline{\boldsymbol{\psi}}^{\mathrm{t}}$. The detailed expressions can be found in [14].

#210984 - $15.00 USD Received 28 Apr 2014; revised 13 Jun 2014; accepted 14 Jun 2014; published 24 Jun 2014

We add all the total residues for each incidence Δ_p^{tot}, $p = 1, 2, ..., N_{\text{inc}}$ together and the unknown matrix $\overline{\overline{O}}$ can be obtained by minimizing the following cost function,

$$f(\overline{\overline{O}}) = \frac{1}{2}\sum_{p=1}^{N_{\text{inc}}} \Delta_p^{\text{tot}}. \tag{6}$$

The optimization steps of cost function in Eq. (6) are similar to that in [14], i.e. the amplitude of induced multipoles $\overline{\mathbf{a}}$ and the *T*-matrices $\overline{\overline{O}}$ are alternatively updated by the two-step conjugate gradient method. We omit the details here and refer the readers to [14] for detail.

Attentions should be paid to the choice of truncation number of multipoles M in the inversion. It is noted that the number of unknowns (dimension of matrix $\overline{\overline{O}}$) is proportional to the truncation order of multipoles M .On the other hand, it is clear that the larger is the truncation number for multipoles M , the more accurate is the calculated scattered field in the *T*-matrix method. Therefore a study of the minimum value of M is critical in ensuring a balance between the accuracy of the solution and the computational cost.

As the fine meshing taken, the size of each subunit is much smaller than the wavelength. Thus, the higher order multipoles decay very fast. In this case, the monopole element is the leading term in *T*-matrices for both PEC and dielectric scatterers. $M = 0$ should be sufficient enough to represent the scattering effect on either the dielectric or the PEC subunits. However it is not accurate to describe the scattering effect of PEC and dielectric together. This is because the monopole element in *T*-matrix for dielectric is compatible in amplitude to the dipole term in *T*-matrix for PEC, and they are on the same order of $k_0 R$ [14]. Thus in the mixed boundary SOP, $M = 1$ should be chosen as the minimum truncation order of multipoles, to accurately represent the scattering effects on both the PEC and dielectric subunits. Detailed derivation of the minimum truncation order can be found in [14].

3.1.2 The scheme of SOP-homo for *T*-matrix method

In this part we indicate how to combine the SOP-homo method with the *T*-matrix inversion method. A mathematical reformulation to the objective function is adopted to further reduce the number of unknowns. Meanwhile, as we treat the 'separable' obstacle as a 'known scatterer', the parameters in the field and state equations remain as the analytical form in free space. We split the objective function into three parts: the field residue $\left(\Delta_{p,n}^{\text{fie}}\right)$, the state residue corresponding to the obstacle subunits $\left(\Delta_{p,n}^{\text{sta}}\right)^{\text{obs}}$ and the state residue corresponding to the non-obstacle subunits $\left(\Delta_{p,n}^{\text{sta}}\right)^{\text{non-obs}}$, i.e.,

$$f\left[\left(\overline{\overline{O}}_n\right)_i\right] = \frac{1}{2}\sum_{p=1}^{N_{\text{inc}}}\left(\frac{\Delta_{p,n}^{\text{fie}}}{\left\|\overline{E}_p^{\text{sca}}\right\|^2} + \sum_{i=1}^{(2M+1)N_{\text{w}}}\frac{\left(\Delta_{p,n}^{\text{sta}}\right)_i^{\text{obs}}}{\left\|\overline{\mathbf{a}}_p^{\text{s}}\right\|^2} + \sum_{i=1}^{(2M+1)(N-N_{\text{w}})}\frac{\left(\Delta_{p,n}^{\text{sta}}\right)_i^{\text{non-obs}}}{\left\|\overline{\mathbf{a}}_p^{\text{s}}\right\|^2}\right). \tag{7}$$

On the right hand side of Eq. (7), the first two terms are constant with respect to the unknowns (the non-obstacle elements). Thus, when updating the matrix $\overline{\overline{O}}$ we only need to update the third term which contains the unknowns, i.e. $\overline{\overline{O}}_i$, $i = 1, 2, ..., (2M+1)(N - N_{\text{w}})$. This manipulation is the key procedure of SOP-homo. It is noted that the *T*-matrices of obstacle components are all fixed during the optimization, while the corresponding amplitudes of the induced multipoles are still being updated.

#210984 - $15.00 USD Received 28 Apr 2014; revised 13 Jun 2014; accepted 14 Jun 2014; published 24 Jun 2014

3.2 The classification procedure

After $\overline{\overline{O}}$ is retrieved by the first step of optimization process, the retrieved *T*-matrix for the *i*th cell is expressed as $\overline{\overline{T}}_i$, $i = 1, 2, ..., N$, which includes both the monopole element $[T]_0$ and dipole elements $[T]_{\pm 1}$. Here we further study the elements in *T*-matrices for PEC and dielectric scatterers, to provide a criterion for differentiating the PEC and dielectric subunits.

We know that the analytical form of monopole element in the *T*-matrix for PEC subunit is $[T]_0 = -\frac{J_0(k_0 R)}{H_0^{(1)}(k_0 R)}$ [22], where $H_0^{(1)}(k_0 R) = J_0(k_0 R) + \mathrm{i} Y_0(k_0 R)$. Under the small term assumption $k_0 R << 1$, $J_0(k_0 R)$ approaches to one, and $Y_0(k_0 R)$ approaches to negative infinity. Therefore, the imaginary part of $[T]_0$ is a negative real number.

The elements of *T*-matrix for dielectric scatterer is nonlinear with respect to ε_{r}. Under the small term assumption $k_0 R << 1$, the monopole element for dielectric subunit can be approximated by the linear polynomial [14],

$$[T]_0 = \frac{\pi (k_0 R)^2}{4\mathrm{i}} (1 - \varepsilon_{\mathrm{r}}). \tag{8}$$

In this paper, we consider only dielectric scatterers, the real part of the relative permittivity of which is larger than one. Thus from Eq. (8), we see that the imaginary part of $[T]_0$ for a dielectric scatterer is larger than zero, which automatically yields the range out of the PEC scatterer.

In summary, for the *i*th subunit, $i = 1, 2, ..., N$, if the imaginary part of $[T]_0$ is positive, the subunit is determined to be dielectric scatterer. While if the imaginary part of $[T]_0$ is negative, the subunit is determined to be PEC. Then the relative permittivity for the dielectric elements can be linearly retrieved from Eq. (8) as,

$$\varepsilon_{\mathrm{r}} = 1 - \frac{4\mathrm{i}[T]_0}{\pi (k_0 R)^2}. \tag{9}$$

3.3. Discussion

This article indicates a special kind of inhomogeneous background detection problem—MB-SOP. In order to solve the MB-SOP, we proposed the new SOP-homo optimization scheme which is adjusted to fit the modeling scheme of *T*-matrix. The proposed optimization method shares several similarities with the original SOP-homo in the following aspects: 1) The cost functions of both methods are reformulated according to the prior information of the separable obstacle. 2) The iterative procedures are similar for the two methods.

Meanwhile, the proposed method essentially differs from the original SOP-homo in the following aspects: 1) The modeling schemes are different. In the original SOP-homo, the EFIE is chosen as the modeling scheme and the relative permittivity is the unknown physical parameter representing the dielectric scatterer. In comparison, in the MB-SOP, the modeling scheme is the *T*-matrix method and the *T*-matrix serves as the unified physical parameter representing both the dielectric and PEC scatterers. 2) The number of unknowns in the original SOP-homo equals to the number of subunits inside the domain. In comparison, the number of unknowns in MB-SOP equals to the number of subunits inside the domain multiplied by the number of truncated multipoles used in the *T*-matrix, which is a compromise of accuracy due to the mixed boundary effect. 3) The original SOP-homo only requires one iterative procedure due to the fact that the scatterers and obstacles are known to be dielectric *a priori*. While the proposed method requires another procedure except for the

#210984 - $15.00 USD Received 28 Apr 2014; revised 13 Jun 2014; accepted 14 Jun 2014; published 24 Jun 2014

iterative procedure to identify the electromagnetic properties of scatterers, which is the essence in solving the MB-SOP.

4. Numerical examples

In this section, we provide three numerical examples to validate our method. The domain of interest for all the numerical examples is square of size $2\lambda \times 2\lambda$, which is discretized into $N = 45 \times 45$ square subunits. $N_{\text{inc}} = 10$ plane incident waves are used to evenly illuminate the domain around a circle. $N_{\text{r}} = 30$ receivers are symmetrically placed around a circle of radius 5λ. The synthetic data are obtained by *T*-matrix method with $M = 2$ and 10% white Gaussian noise is added. In the inversion, $M = 1$ is the truncation number of the multipoles. Because the dipole term of *T*-matrix does not numerically exist for $\varepsilon_{\text{r}} = 0$, in order to present both PEC and dielectric subunits uniformly, we use $\varepsilon_{\text{r}} = 0$ to mark the PEC scatterers in the relative permittivity profiles. It should be noted that this is only an artificial representation which have no actual physical meaning.

4.1 Example one

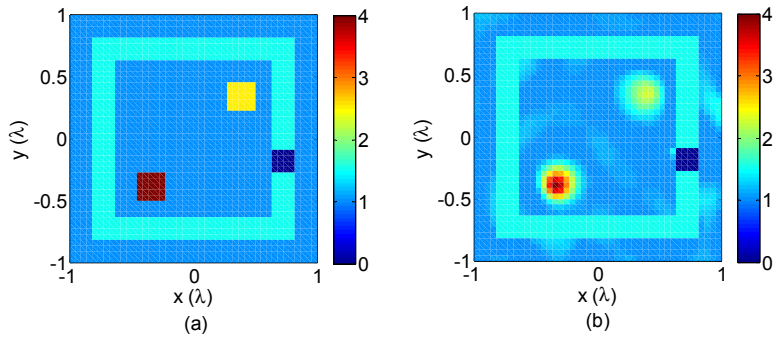

Fig. 2. The configuration of scatterers in the first example. The scattering data are contaminated with 10% white Gaussian noise. (a) Exact profile. (b) Reconstructed profile.

As shown in Fig. 2(a), in the first example the obstacle which encloses the unknown scatterers is square shaped, with the outer side length 1.63λ and the inner side length 1.26λ. The relative permittivity of obstacle is 1.5. There is one square metallic rod embedded in the right part of the obstacle. Two square unknown scatterers are enclosed inside the obstacle, with the relative permittivities of 2.5 and 4 respectively.

The reconstruction pattern is shown in Fig. 2(b), where the two dielectric scatterers are clearly recognized even with the PEC obstacle presenting. The relative permittivities for the two scatterers are also well reconstructed. The result is quite satisfactory considering the complex experimental setup and the noise level.

#210984 - $15.00 USD Received 28 Apr 2014; revised 13 Jun 2014; accepted 14 Jun 2014; published 24 Jun 2014

4.2 Example two

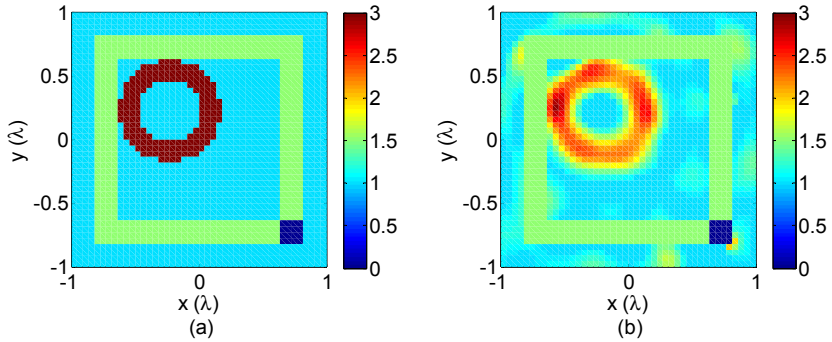

Fig. 3. The configuration of scatterer in the second example. The scattering data are contaminated with 10% white Gaussian noise. (a) Exact profile. (b) Reconstructed profile.

In the second example, a more complicated unknown scatterer is used to test the resolution of the proposed method. An annulus ring structure is commonly considered difficult to be reconstructed in the inverse scattering society. In this example, the unknown scatterer is an annulus scatterer with outer radii 0.4λ and inner radii 0.25λ. The scatterer is placed adjacent to the obstacle as shown in Fig. 3(a). The relative permittivity of the annulus is 3. The shape and relative permittivity of the obstacle remain the same as the first example except that the square PEC rod is in the right down corner.

From the reconstruction result as shown in Fig. 3(b), we can see that despite the existence of the PEC rod and the strong interaction between the PEC rod and dielectric annulus, the annulus shaped scatterer is still successfully reconstructed with the hole clearly seen in the middle. Because the obstacle components are fixed during the optimization, even though the obstacle and scatterer are adjacent to each other, they can still be clearly separated in the reconstruction pattern. This is a significant advantage of the SOP-homo over the tradition methods for the inhomogeneous background problem [13].

4.3 Example three

In the third example, we test the algorithm for mixed boundary obstacle as well as the mixed boundary scatterers, where the unknown scatterers to be reconstructed are consisted by both the PEC and dielectric scatterers. The obstacle remains the same as example two. There are two scatterers placed inside the domain of interest as shown in Fig. 4(a), one of which is a square dielectric scatterer with $\varepsilon_r = 4$ and the other is a square shaped PEC scatterer.

From the reconstructed pattern as shown in Fig. 4(b), we can clearly see the PEC scatterer and the dielectric scatterer. The positions and the properties of the scatterers are well reconstructed.

#210984 - $15.00 USD Received 28 Apr 2014; revised 13 Jun 2014; accepted 14 Jun 2014; published 24 Jun 2014

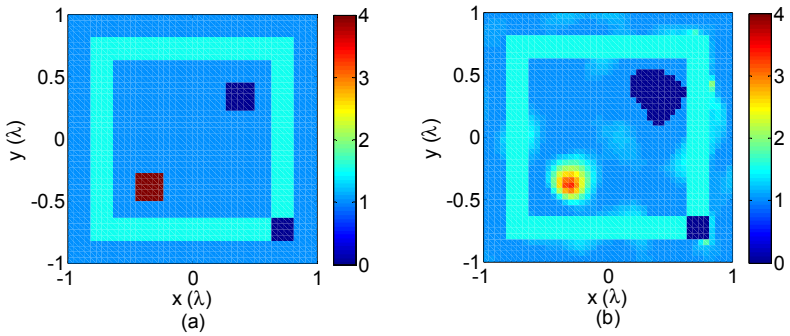

Fig. 4. The configuration of scatterer in the third example. The scattering data are contaminated with 10% white Gaussian noise. (a) Exact profile. (b) Reconstructed profile.

5. Conclusion

This article indicated a special kind of inhomogeneous background detection problem—MB-SOP, where the obstacles are separable from the unknown scatterers and both the obstacle and the scatterers are consisted by mixture of dielectric and PEC materials. In order to solve the MB-SOP, the *T*-matrix modeling scheme is introduced to describe both the PEC and dielectric together and the optimization scheme SOP-homo is successfully combined with the framework of *T*-matrix. The optimization scheme successfully utilized the prior information of separable obstacle. Thus, no numerical calculation of the inhomogeneous background Green's function is involved. The elements corresponding to obstacle media are excluded from the updating process of *T*-matrices to further reduce the computational cost. Finally, a classification criterion in differentiating the PEC and dielectric subunits is provided according to element analysis in *T*-matrix. Numerical results indicate that the *T*-matrix SOP-homo is an effective method in solving the MB-SOP and is quite robust against noise.

#210984 - $15.00 USD Received 28 Apr 2014; revised 13 Jun 2014; accepted 14 Jun 2014; published 24 Jun 2014